Available online at www.sciencedirect.com
ScienceDirect
Journal of Power Sources 173 (2007) 77–85
JOURNAL OF POWER SOURCES
www.elsevier.com/locate/jpowsour

Cathode electrocatalyst selection and deposition for a direct borohydride/hydrogen peroxide fuel cell

Lifeng Gu *, Nie Luo, George H. Miley

Department of Nuclear, Plasma and, Radiological Engineering, University of Illinois at Urbana-Champaign, Urbana, IL 61801, USA

Received 13 April 2007; received in revised form 2 May 2007; accepted 3 May 2007
Available online 7 May 2007

Abstract

Catalyst selection, deposition method and substrate material selection are essential aspects for the design of efficient electrodes for fuel cells. Research is described to identify a potential catalyst for hydrogen peroxide reduction, an effective catalyst deposition method, and supporting material for a direct borohydride/hydrogen peroxide fuel cell. Several conclusions are reached. Using Pourbaix diagrams to guide experimental testing, gold is identified as an effective catalyst which minimizes gas evolution of hydrogen peroxide while providing high power density. Activated carbon cloth which features high surface area and high microporosity is found to be well suited for the supporting material for catalyst deposition. Electrodeposition and plasma sputtering deposition methods are compared to conventional techniques for depositing gold on diffusion layers. Both methods provide much higher power densities than the conventional method. The sputtering method however allows a much lower catalyst loading and well-dispersed deposits of nanoscale particles. Using these techniques, a peak power density of 680 mW cm^{-2} is achieved at 60 °C with a direct borohydride/hydrogen peroxide fuel cell which employs palladium as the anode catalyst and gold as the cathode catalyst.

Keywords: Direct borohydride/hydrogen peroxide fuel cell; Pourbaix diagram; Gold catalyst; Sputtering deposition; Activated carbon cloth

1. Introduction

Methanol and sodium borohydride are important fuel candidates for portable and mobile applications at ambient temperature. Direct borohydride fuel cells provide higher open circuit voltages and higher power densities than both hydrogen/oxygen fuel cells and direct methanol fuel cells. Hence they have received increasing attention starting in 2000 [1–3].

There is considerable motivation to use H_2O_2 in place of O_2 at the cathode to achieve even better performance and air independence for applications such as space power and underwater operation. The resulting system is termed a direct sodium borohydride/hydrogen peroxide fuel cell (DBHPFC).

Oxygen reduction at the cathode of a PEM fuel cell is:

$$O_2 + 4H^+ + 4e^- \rightarrow 2H_2O \quad (1)$$

This reaction involves simultaneous transfer of four electrons, and therefore has a reduced probability of occurrence [2,4]. It is known that the exchange current density of oxygen reduction is 6 orders of magnitude lower than that of hydrogen oxidation [4–7]. The slow kinetics of oxygen reduction limits the power density and cell efficiency. In comparison, the reduction reaction of hydrogen peroxide is:

$$H_2O_2 + 2H^+ + 2e^- \rightarrow 2H_2O \quad (2)$$

This is a two-electron transfer process and hence has lower activation over potential than four-electron transfer process. So fuel cell systems using hydrogen peroxide as the cathode fuel tend to provide higher performance than systems using oxygen. In addition, hydrogen peroxide has other advantages. Its liquid form makes the system more compact and convenient. It is environmentally friendly and easy to handle. Its wide application and high volume production make it a low cost product in current market.

Many factors are involved in the cell optimization issue. Catalyst selection is always a critical one, especially in a cell like DBHPFC where less explored fuels are involved. Indeed exten-

* Corresponding author. Tel.: +1 2177219195; fax: +1 2173332906.
E-mail address: lgu2@uiuc.edu (L. Gu).

0378-7753/$ – see front matter © 2007 Elsevier B.V. All rights reserved.
doi:10.1016/j.jpowsour.2007.05.005

sive research effort has been put on the development of catalysts for different kinds of fuel cells since the first hydrogen/oxygen fuel cell. The objective of the research described here was to identity a potential catalyst for hydrogen peroxide reduction and to address an effective catalyst supporting material and catalyst deposition method for this all liquid fuel cell. The anode catalyst selection is also equally important and its research is described elsewhere.

2. Direct borohydride/hydrogen peroxide fuel cell

2.1. Cell structure

Fig. 1 shows an assembled DBHPFC that has been used in extensive testing. Its structure and materials selection are made for ease of use in the laboratory where components are frequently interchanged. Later models will generally follow this design, but will use optimized materials.

Graphite is used as the bipolar plate material. A serpentine style is employed, which is shown in Fig. 2 [8]. The flow rates are low so the pressure drop with this design remains manageable. A small pump is used to control the fuel flowing through the channel.

Nafion is employed as the exchange membrane. Since liquid fuels are used in the cell system, humidification problems associated with PEM fuel cells are avoided. The selection of the porous and conductive material used as the diffusion layer, the catalyst and its deposition on the diffusion layer are discussed later.

2.2. Operation system

Figs. 3 and 4 illustrate the schematic diagram and the operation system of the DBHPFC. NaOH was added to the anode solution to stabilize $NaBH_4$, inhibiting its hydrolysis reaction.

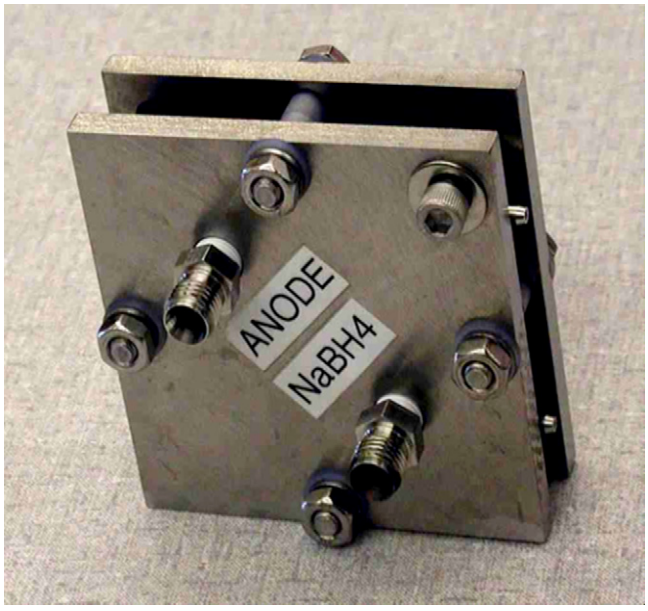

Fig. 1. Assembled DBHPFC test unit.

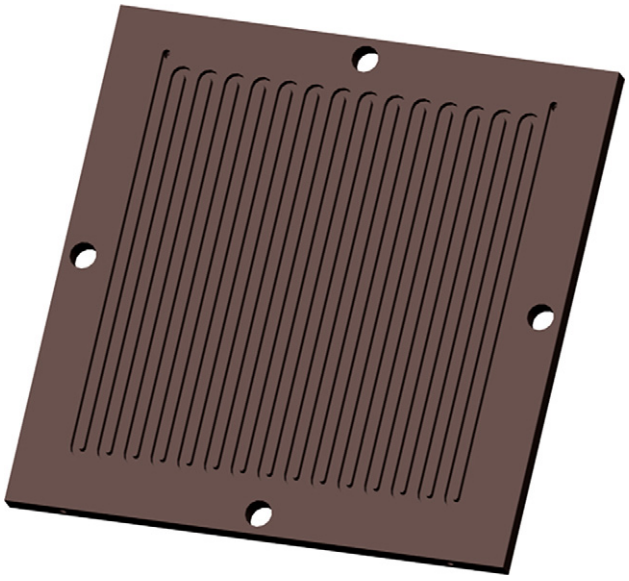

Fig. 2. Serpentine bipolar plate.

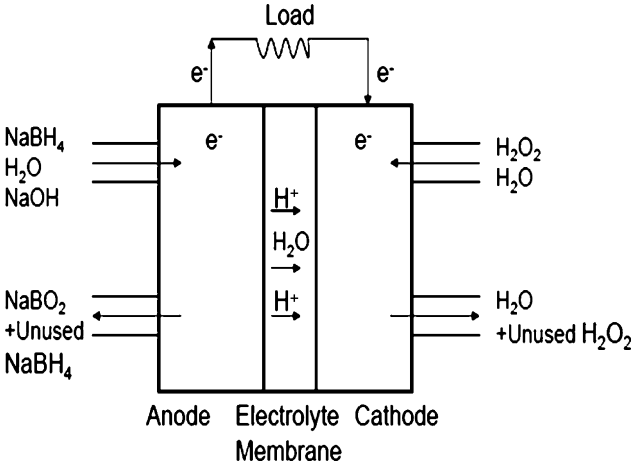

Fig. 3. Schematic diagram of the DBHPFC.

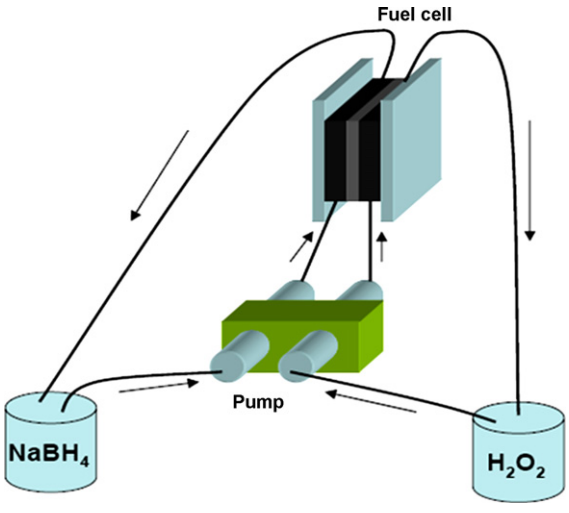

Fig. 4. Operation system of the DBHPFC.

Sodium borohydride solution is pumped into the serpentine channels at the anode, diffuses through the diffusion layer and reacts with water under the anode catalyst. The half reaction is:

$$NaBH_4 + 2H_2O \rightarrow NaBO_2 + 8H^+ + 8e^-, \quad E^\circ = -0.471\,V \tag{3}$$

The reaction products are sodium metaborate, protons and electrons. The protons transport through the exchange membrane to the cathode while the electrons travel along the external circuit to the cathode. There they both react with hydrogen peroxide under a specific catalyst. The half reaction is:

$$4H_2O_2 + 8H^+ + 8e^- \rightarrow 8H_2O, \quad E^\circ = 1.776\,V \tag{4}$$

During cell operation, water is dragged from the anode to the cathode through the membrane by protons via electro-osmotic drag. This drag effect and the consumption of water by the chemical reaction at the anode combine to cause a loss of water at the anode. Hence solubility for sodium borohydride and sodium metaborate ultimately limits the run time for the closed cycle operation system. The maximum concentration of sodium borohydride solution that can be used in the system is limited by the solubility of sodium borohydride at specific temperature.

2.3. Electrocatalysts for the DBHPFC

Catalysts play a critical role in defining the performance of a fuel cell. The specific requirements depend on the type of fuel cell involved. The catalyst selection criteria for the DBHPFC are discussed here.

First, electrocatalysts must provide high catalytic activities for electrochemical oxidation of $NaBH_4$ at the anode and electrochemical reduction of H_2O_2 at the cathode. Second, candidate materials should have good stability towards corrosion. Third, good electrical conductivity is needed to minimize the resistive loss in the catalyst layer. Fourth, direct oxidization of sodium borohydride to H^+ is desired. However, sodium borohydride can react with water to form hydrogen gas:

$$NaBH_4 + 2H_2O \rightarrow 4H_2 + NaBO_2 \tag{5}$$

If hydrogen gas is produced instead of protons, sodium borohydride fuel will be wasted, resulting in low fuel efficiency. Theoretically, one ion of BH_4^- can generate eight electrons. However, in real systems, the number of electrons actually utilized per ion of BH_4^- oxidized is less than eight since reaction (3) has to compete with hydrolysis reaction (5). The actual reaction can be written as:

$$NaBH_4 + 2H_2O \rightarrow NaBO_2 + xH^+ + (4 - \tfrac{1}{2}x)H_2 + xe^- \tag{6}$$

Here x denotes the actual number of electrons released by each BH_4^- ion and is called columbic efficiency. The most influential factor in the determination of x is the electrocatalyst. Research indicated that Au anode electrode demonstrated high columbic efficiency (6.9 electrons per molecule of BH_4^-) [9,10]. Palladium was identified as the anode catalyst for the UIUC DBHPFC by experimental study. Our experiments showed that Au was better than Pd by further decreasing hydrogen evolution, but the catalytic reaction of Au was lower in terms of power generated by the cell.

Last but not the least, direct reduction of hydrogen peroxide is desired. At the cathode, hydrogen peroxide can spontaneously decompose exothermically into water and oxygen gas [11]:

$$2H_2O_2 \rightarrow 2H_2O + O_2 \tag{7}$$

This process is very favorable and occurs at temperatures above the melting point of the solution. The rate of decomposition increases as the temperature increases. The direct reduction of hydrogen peroxide is shown in reaction (4). If oxygen gas is generated during cell operation, hydrogen peroxide fuel will be wasted, reducing the fuel efficiency. In addition, ultimately the present fuel cell is to be designed as a sealed unit, so gas evolution is undesirable.

Little literature exists pertaining to the catalyst development for direct hydrogen peroxide reduction. Raman et al. have demonstrated a direct borohydride/hydrogen peroxide fuel cell using Pt/C as the cathode catalyst and AB_5 metal hydrogen storage alloy as the anode catalyst and achieved 350 mW cm^{-2} at 343 K [12]. An approach in which Pourbaix diagrams are employed to guide the catalyst selection for hydrogen peroxide reduction is described in the following section.

3. Catalyst selection for hydrogen peroxide reduction

3.1. Catalyst selection using Pourbaix diagrams

Pourbaix diagrams depict the thermodynamical form of an element as a function of potential and pH of a given environment [13]. These diagrams provide a visual representation of the oxidizing and reducing abilities of the major stable compounds of an element. They are frequently used in material studies for environmental applications. Here these diagrams are used to identify a potential catalyst that can minimize cathode gas evolution of the DBHPFC during cell operation. Fig. 5 [13] is the Pourbaix diagram for the hydrogen peroxide–water system at 25 °C.

The lines (a and b) in the diagram are the stability and redox lines of water. Below the family of lines 2–3, H_2O_2 is unstable and is rapidly reduced to water according to the reaction:

$$H_2O_2 + 2H^+ + 2e^- \rightarrow 2H_2O \tag{8}$$

Above the family of lines 4–5, H_2O_2 becomes unstable again and acts as a reducing agent with the formation of oxygen gas. This chemical reaction is:

$$H_2O_2 \rightarrow O_2 + 2H^+ + 2e^- \tag{9}$$

The region below the family of lines 2–3 and the region above the family of lines 4–5 have a common area, where H_2O_2 is doubly unstable and can rapidly decompose into oxygen and water:

$$2H_2O_2 \rightarrow O_2 + 2H_2O \tag{10}$$

When H_2O_2 solution is in contact with a metallic surface whose electrode potential lies in the region of double instability, H_2O_2 will spontaneously decompose into oxygen and water [13]. On

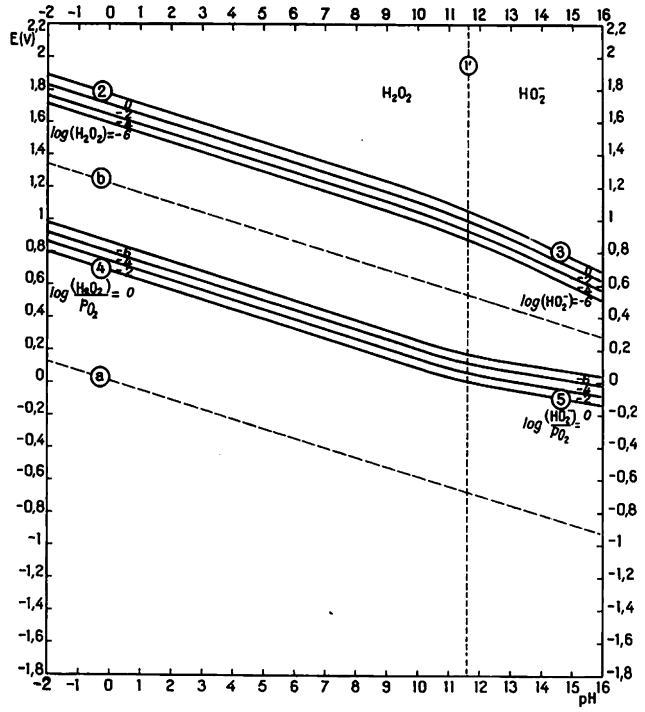

Fig. 5. Pourbaix diagram of the H_2O_2–water system at 25 °C.

the other hand, if the electrode potential of the metallic surface falls outside of this region, decomposition will not occur. And if the electrode potential of the metallic surface falls to the region close to the family of lines 2–3, then reaction (8) will be the dominant reaction. This insight is very helpful for selecting a proper catalyst for direct hydrogen peroxide reduction.

The pH value of the hydrogen peroxide solution used in our experiments is zero, so the electrode potential varies from 0.70 to 1.80 V in the region of double instability. Mean value is 1.25 V. In order to avoid or minimize H_2O_2 decomposition, the catalyst electrode potential must be out of this range or fall to the region close to the family of lines 2–3. The choice was first narrowed down to the noble metals due to their good catalytic ability and good stability towards corrosive environments since hydrogen peroxide is a powerful oxidizer. The task of catalyst selection then is to identify one or more noble metals that have the desired electrode potential.

The redox information of noble metals can be obtained from their Pourbaix diagrams. Fig. 6 is a simplified version of Pourbaix diagrams for gold, silver, platinum, palladium, ruthenium, rhodium, osmium and iridium [14]. The white area in the diagrams is the stable domain of natural water. The lines in each Pourbaix diagram separate species in redox equilibrium as a function of potential and pH. The chemical formula of the predominant substances in each region is also displayed. The oxides of these elements are not considered as catalyst candidates because they will react with H^+ in acid environment. So here the redox equilibrium lines between the metal and its closest oxide are of major interest.

By comparing the diagrams in Fig. 6 with the diagram in Fig. 5, it can be seen that each of the eight metals has its redox equilibrium line between the metal and its closest oxide in the domain of double instability of hydrogen peroxide. Also platinum, ruthenium, rhodium, osmium, iridium, silver and palladium have their equilibrium lines close to the lower boundary or the center of the domain, a favorable condition for the oxidization of H_2O_2 into oxygen. This shows these metals are good catalysts for the decomposition of H_2O_2 but this is undesirable for our present use. For example, the potential value for the reaction $Pt \rightarrow Pt^{2+} + 2e^-$ when pH is 0 is 1.20 V. This is very close to the mean value of 0.70 and 1.80 V (1.25 V). So when H_2O_2 solution contacts Pt, gaseous oxygen is easily seen forming on the metal surface.

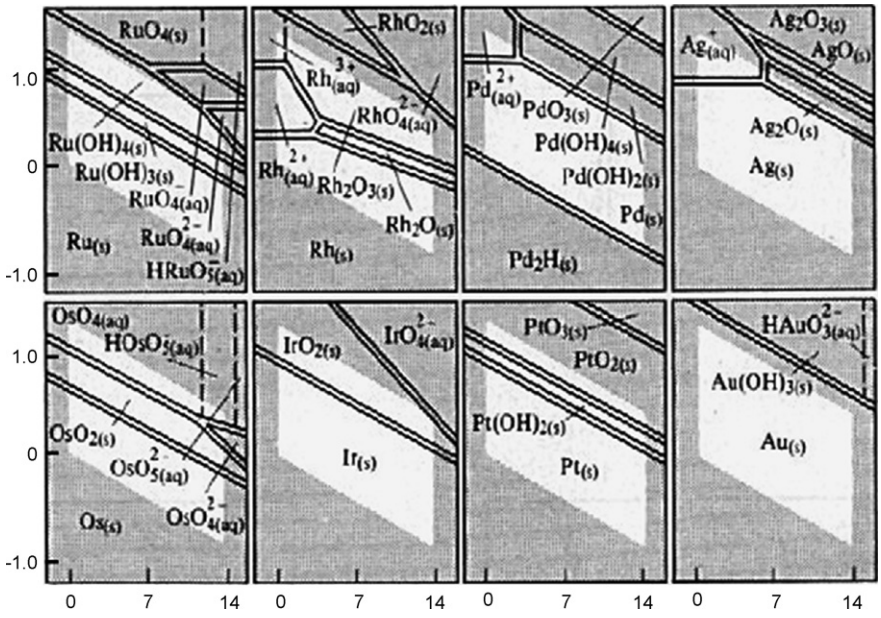

Fig. 6. Simplified Pourbaix diagrams of noble metals: gold (Au), silver (Ag), platinum (Pt), palladium (Pd), ruthenium (Ru), rhodium (Rh), osmium (Os) and iridium (Ir).

However, it is also observable that the redox equilibrium lines of gold are very close to the upper boundary of the domain. This is a favorable condition for the reduction of hydrogen peroxide into water according to the reaction (8). So for the noble metals included, this analysis predicts that gold provides the most complete reduction of hydrogen peroxide. While there may be other possibilities, including alloys, gold was then selected here for experimental study as described next.

3.2. Experimental results

Experiments were performed to check the gas production predictions by placing samples of the above listed metals into hydrogen peroxide solution with the same concentration (30 wt.%) and pH value. A large amount of oxygen gas was noticed on the surface of platinum, ruthenium, rhodium, osmium, iridium, silver and palladium. But gas bubbling was not noticeably visible when gold was placed into hydrogen peroxide solution. This experimental result is consistent with the theoretical prediction using Pourbaix diagrams.

In order to verify that gold catalyst provides sufficient reactivity for use in a fuel cell, power curves were obtained by operating DBPHFC at room temperature with each of these metal catalysts on the cathode. The anode catalyst, the anode fuel and the cathode fuel were kept identical in all cases. Palladium was used as the anode catalyst. The anode fuel consisted of 10 wt.% sodium borohydride, 5 wt.% sodium hydroxide and 5 wt.% ammonium hydroxide in water. The purpose of ammonium hydroxide is to help resolve the reaction product $NaBO_2$. The cathode fuel was 10 wt.% hydrogen peroxide and 5 wt.% phosphoric acid in water. Results are presented in Fig. 7. The purpose of phosphoric acid is to help stabilize H_2O_2.

Although gold does not show the best power density in Fig. 7, it shows a relatively good power density. While Pd and Os offered slightly higher power densities, significant gas production was observed, consistent with the earlier static tests. The formation of oxygen gas results in a reduction in H_2O_2 fuel efficiency, which offsets the power density advantage. Further, gas production cannot be allowed in a closed cell configuration. In summary, these results support the conclusions drawn from the Pourbaix diagram analysis that Au is the preferred cathode catalyst. However, only noble metals have been considered to date. Other materials such as alloys will be evaluated in the future.

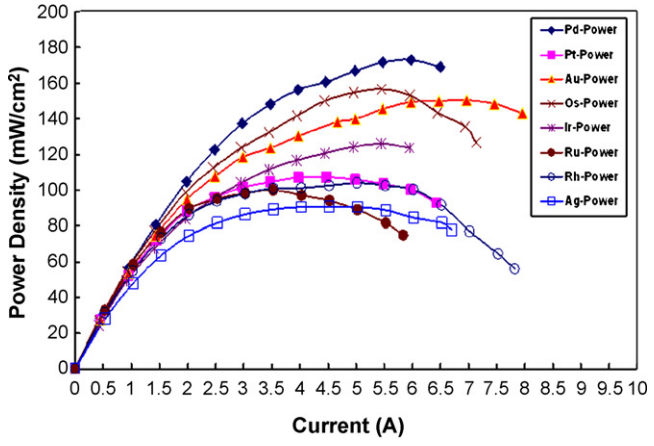

Fig. 7. Cathode catalyst performance comparison.

4. Catalyst supporting material

In principle, the fine dispersion and desired catalyst particle size can be obtained by adopting an appropriate preparative procedure on an ideal supporting material [15,16]. That is to say, by selecting good supporting material, a finer catalyst deposition pattern and better electrode performance can be achieved. Commonly used catalyst support materials are carbon related products such as carbon power, carbon paper and carbon cloth. High surface area carbon powder is reported to provide good catalyst support and this high surface feature helps to obtain relatively higher power densities. However, the complex deposition procedures associated with carbon powder and its relatively poor adhesion hampers its use.

Activated carbon cloth which denotes a material that has an exceptionally high surface area, and includes a large amount of microporosity (Fig. 8) is an ideal choice for catalyst support. A high surface area of the supporting material provides the catalyst particles with a huge number of deposit sites, which helps those particles to widely disperse on the surface of the support. And eventually, a more uniform distribution and smaller size particles can be produced.

Activated carbon cloth with an activation level of 2000 $m^2\ g^{-1}$ was chosen to be the supporting material for gold deposits using electrodeposition and sputtering methods discussed in the next section. Both methods achieved a high power level with this substrate material.

Further, some improvement might be possible in the future using cloth with an even higher activation level. However, as the activation level increases, the pore radius increases. This may result in a low electrical conductivity which will adversely affect the performance of the cell. So there is a trade-off between activation level and electrical conductivity. Further experiments are needed to explore this issue.

5. Catalyst deposition methods

In addition to catalyst selection and substrate material, electrode performance strongly depends on the structure and fabrication of the catalyst layer. Catalyst deposition directly impacts the catalytic activity by determining the size of catalyst particles and their dispersion over the supports [17,18]. A catalyst layer with a lowest level of loading required to achieve a fixed power level will reduce catalyst costs which is one of the major components in fuel cell cost.

5.1. Conventional deposition techniques

Since the application of PEM fuel cells in Gemini space flights in the 1960s, a significant amount of research work has been done on the electrode design for PEM fuel cells using various catalyst deposition methods [19–21]. Conventional deposition method is a method in which catalyst particles

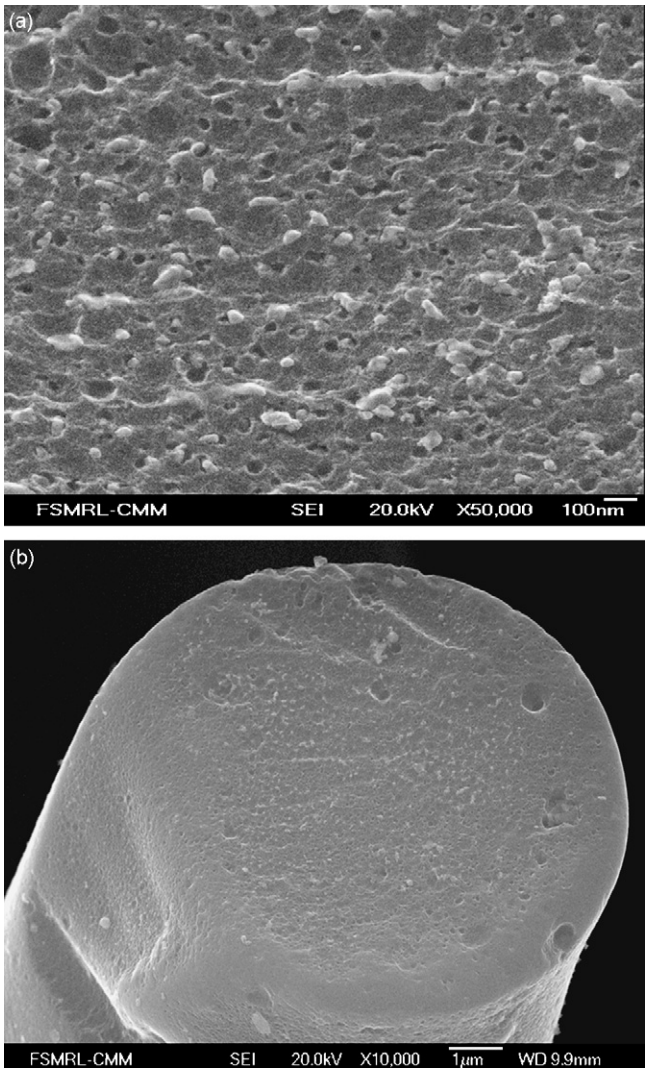

Fig. 8. Scanning electron micrograph of microporous structure of the activated carbon fiber.

mixed with Nafion solution are applied to the diffusion layer. This method was also employed to fabricate the catalyst layers in our original DBHPFC. The procedures are as follows:

(1) Combine a 5 wt. % Nafion solution and 99.9 wt.% palladium black in a weight ratio of 1:1 Nafion/Pd.
(2) Add methanol to achieve a weight ratio of 1:1:20 Nafion–Pd–methanol.
(3) Mix the solution with homogenizer for 30 min.
(4) Apply the catalyst ink to one side of the carbon cloth diffusion layer. Typically several coats are required for adequate level of catalyst loading.
(5) Dry the diffusion layer in the oven at 80 °C for 20 min.
(6) Use a high concentration sulfuric acid to treat the diffusion layer.
(7) Take the diffusion layer out of the sulfuric acid solution, rinse it with water and dry it again in the oven at 80 °C for 20 min. The same procedure was employed to fabricate the cathode catalyst layer with a gold black catalyst.

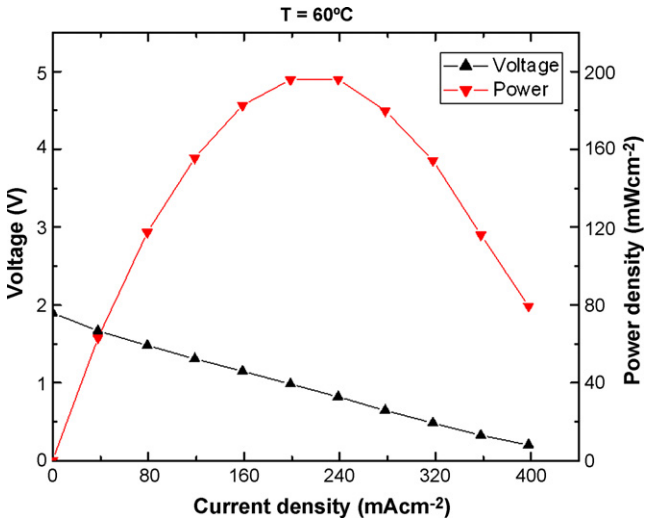

Fig. 9. Testing result of catalyst layers fabricated using conventional deposition method.

The testing result of the catalyst layers fabricated using the above techniques is presented in Fig. 9.

According to Fig. 9, the peak power density generated is 190 mW cm^{-2}, which is similar to the result reported by Choudhury et al. [20]. Thus, there does not appear a significant advantage for the UIUC cell. This is probably due to the low catalyst utilization associated with this conventional deposition method. Yet higher power densities are desired, so it is desirable to develop or employ other deposition methods to improve the catalyst performance.

5.2. *Electrodeposition and sputtering deposition methods*

Electrodeposition and sputtering are two emerging methods for depositing catalysts. Electrodeposition is able to deposit particles in nanometer scale onto the substrates. Also electrodeposition method deposits catalyst where the three-phase zone is located. The diagram of this three-phase zone is shown conceptually in Fig. 10. The catalyst loading is reduced by only depositing catalyst in this zone.

The electrodeposition method has also shown to successfully cover the inner surface of the porous substrates, while most of the other deposition methods fail to do so [18,22]. All these results indicate that electrodeposition method has an excellent potential for achieving effective catalyst layers. What is more, the electrodeposition process is very simple and controllable and the equipment required is inexpensive. These are key advantages for commercial applications.

The sputtering method provides another method of depositing a thin catalyst layer that delivers high performance with low levels of catalyst loadings [23,24]. The success of the sputtering method for reducing the catalyst loading depends heavily on the reduction in the size of catalyst particles [25]. With a given carbon support, reducing the size of catalyst particles will increase the catalyst surface area [2]. Thus, a high level of loading is not needed to provide high surface area in this case. But the performance of a fuel cell with a sputtered catalyst layer can vary,

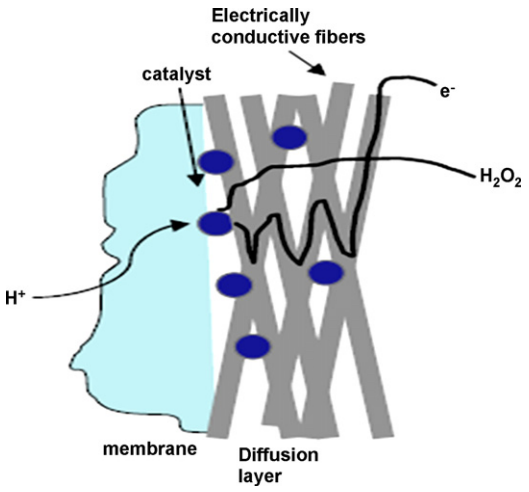

Fig. 10. Diagram of the three-phase zone.

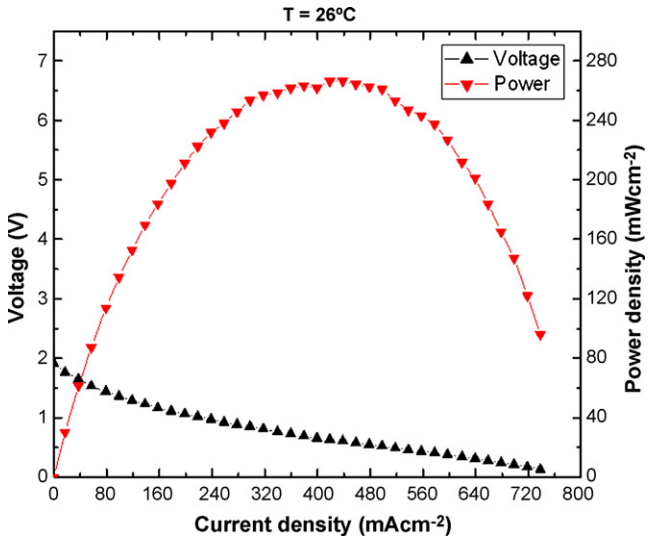

Fig. 11. *V–I* curve and *P–I* curve generated by electrodeposited gold catalyst layer and electrodeposited palladium layer at 26 °C.

widely depending on the thickness of the sputtered catalyst layer [26]. However, uniform and reproducible layers containing low catalyst loadings with this technique offer great potential for achieving an attractive large-scale manufacture.

Both electrodeposition and sputtering methods were employed to apply cathode catalyst on diffusion layers in the UIUC DBHPFC. A gold electrodeposition process was performed using a chloroauric acid plating bath at room temperature. A solution of palladous salts was used to deposit anode catalyst palladium. Then the catalyst layers were tested by operating fuel cell at two different temperatures. In order to compare the results, key conditions were designed to be identical. The concentration of the sodium borohydride solution was 18 wt.% and the concentration of the hydrogen peroxide solution was 17 wt.%. In all tests, only the cathode electrode construction was varied while the anode electrode was kept the same with a palladium catalyst layer deposited using the electrodeposition method. The *V–I* curves and the power-*I* curves of the tests are presented in Figs. 11–14. The peak power densities were summarized in Table 1.

According to Figs. 11–14, a high open circuit voltage (~1.95 V) was obtained in all cases. This confirms that a high catalyst activity was achieved by the catalyst layers fabricated with both electrodeposition and sputtering methods.

According to Table 1, the peak power density at 26 °C is 270 mW cm^{-2} in the electrodeposition case and 240 mW cm^{-2} in the sputtering case. At 60 °C the values are 680 mW cm^{-2} and 600 mW cm^{-2}, respectively. The power densities are much higher than the results reported for such cells in the literature. Also the power densities are higher than those generated by our original cells which have the same cell structure and the same type of catalysts but different catalyst deposition methods. This shows that the electrodeposition and sputtering methods give better performance than the conventional method in terms of power densities.

Table 1
Peak power densities generated by UIUC cell at 26 and 60 °C

	T = 26 °C	*T* = 60 °C
Electrodeposition	270 mW cm^{-2}	680 mW cm^{-2}
Sputtering deposition	240 mW cm^{-2}	600 mW cm^{-2}

In order to obtain more information about catalyst deposition, the surfaces of the electrodes were observed by a JEOL JSM-7000F Field Emission Analytical Scanning Electron Microscope. Figs. 15 and 16 present the scanning electron micrographs of gold deposits using electrodeposition and sputtering deposition, respectively.

Fig. 15 displays a dendritic crystal structure obtained during the electrodeposition process. This structure decreases the surface area of the catalyst and makes the deposit unstable. It is attributed to the large current density used in the electrodeposition process. The current density exerts an important effect on the deposit properties such as size, shape and distribution of the deposit. When the current density reaches the limiting value, the

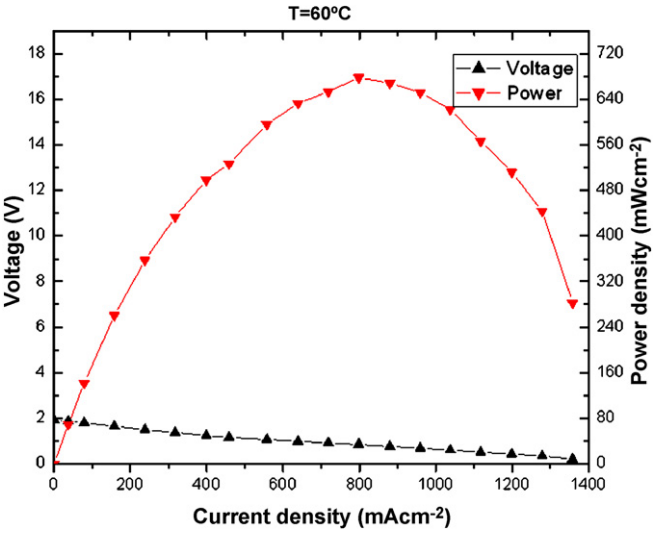

Fig. 12. *V–I* curve and *P–I* curve generated by electrodeposited gold catalyst layer and electrodeposited palladium layer at 60 °C.

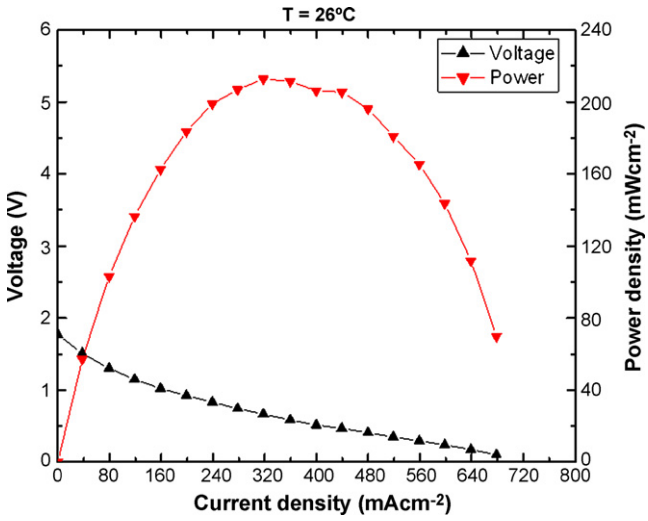

Fig. 13. *V–I* curve and *P–I* curve generated by sputtered gold catalyst layer and electrodeposited palladium layer at 26 °C.

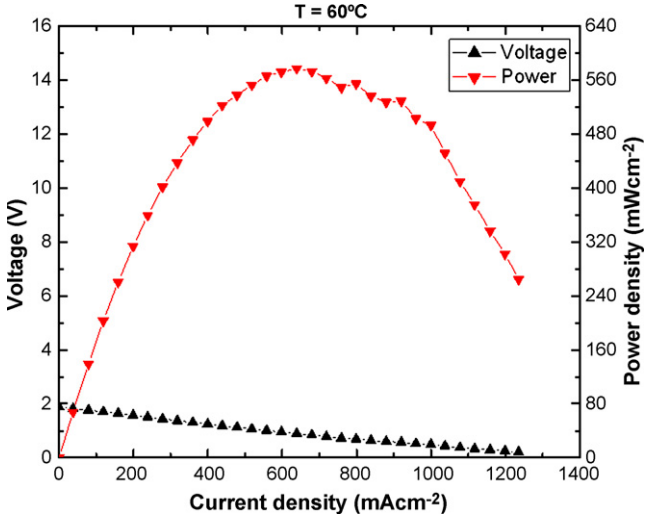

Fig. 14. *V–I* curve and *P–I* curve generated by sputtered gold catalyst layer and electrodeposited palladium layer at 60 °C.

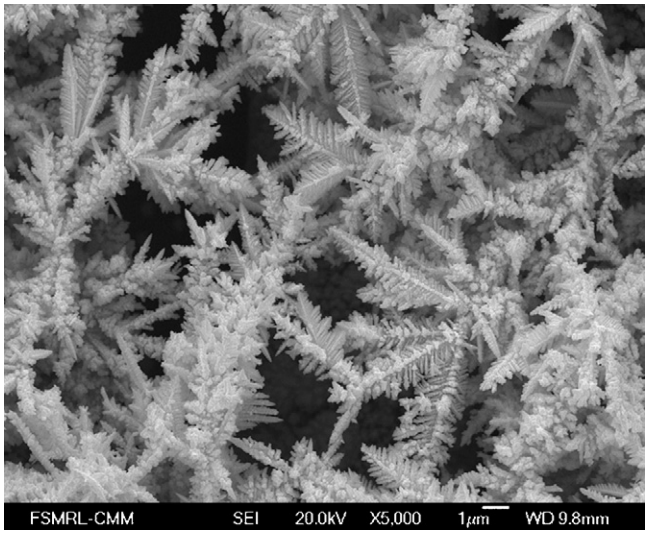

Fig. 15. Scanning electron micrograph of Au deposits using electrodeposition method.

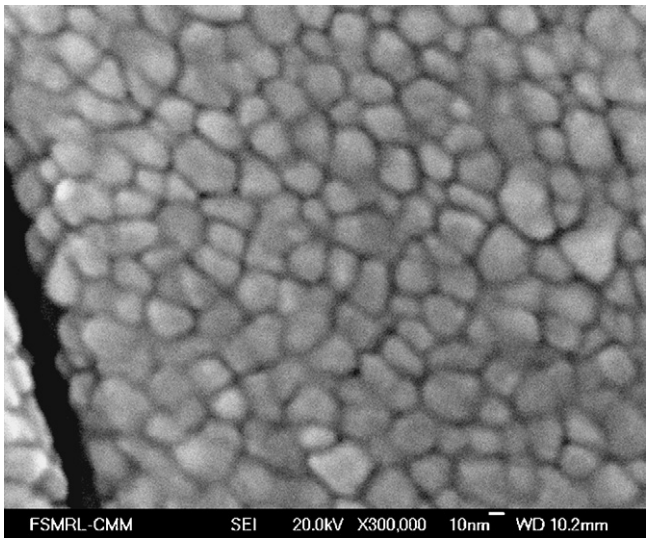

Fig. 16. Scanning electron micrograph of Au deposits using sputtering method.

dendritic crystal structure begins to grow. The present electrodeposition approach is limited to high current densities. Prior to these results, the disadvantage of this was not realized. Instead of developing lower currents, pulsed electrodeposition [26] has been recommended to reduce dendritic structure.

Very uniformly distributed catalyst deposits using sputtering method were formed in Fig. 16. Nanoparticles of an average size of 10 nm were produced. These good features resulted in the excellent power performance of the cell presented in Figs. 13 and 14. The loading of the catalyst deposit is 0.19 mg cm^{-2}, which is much lower than the loading in the electrodeposition case (0.5 mg cm^{-2}). Thus, the sputtering method shows a better performance than the electrodeposition method by sustaining almost the same level of power density while using a much lower catalyst loading.

6. Conclusions

The objective of this paper is to identity a potential catalyst for direct hydrogen peroxide reduction and to address an effective catalyst deposition method and effective catalyst supporting material for the direct borohydride/hydrogen peroxide fuel cell.

By theoretical analysis using Pourbaix diagrams combined with experimental testing, gold was identified as an effective cathode catalyst for the DBHPFC. This catalyst is able to minimize the gas evolution of hydrogen peroxide during cell operation while providing relatively high cell performance. However, only noble metals have been considered to date. Other materials such as alloys might be evaluated in the future.

Activated carbon cloth which features high surface area and microporosity was identified as a promising supporting material for catalyst deposition. However, there is a trade-off between the activation level and electrical conductive ability. Further experiments are needed to explore these issues.

Catalyst layers fabricated by electrodeposition and sputtering methods showed higher open circuit voltages and power den-

sities than catalyst layers fabricated by conventional method. The sputtering method showed better performance than the electrodeposition method by sustaining almost the same level of power density with much lower catalyst loading. This performance is attributing to well dispersed catalyst deposits and nanoscale particles achieved with the plasma sputtering method. Since dendritic growth due to the large current density was not avoided in the electrodeposition case, further improvement in this approach might be made by using other techniques such as pulsed electrodeposition and electrodeposition with bulk convention.

A peak power density of 680 mW cm^{-2} was achieved at 60 °C by UIUC direct borohydride/hydrogen peroxide fuel cell with gold as anode catalyst and palladium as cathode catalyst. This result is higher than power densities reported for fuel cells using these fuels. This improvement is advantageous for eventual commercial applications of the UIUC direct borohydride/hydrogen peroxide fuel cell.

Acknowledgements

The research work was funded by DARPA Contract No. FA9453-05-C-0084 and NASA Contract No. NNC05CB04C. We want to thank James C. Mabon and Tony Banks (MRL, UIUC) for providing valuable technique support.

References

[1] J. Larminie, A. Dicks, Fuel Cell Systems Explained, 2nd ed., Wiley, New York, 2003.
[2] G. Hoogers, Fuel Cell Technology Handbook, CRC Press LLC, 2003.
[3] C. Ponce de Leon, F.C. Walsh, D. Pletcher, D.J. Browning, J.B. Lakeman, J. Power Sources 155 (2006) 172–181.
[4] R. O'Hayre, S.-W. Cha, W. Colella, F.B. Prinz, Fuel Cell Fundamentals, Wiley, New York, 2006.
[5] N. Luo, G.H. Miley, P.J. Shrestha, R. Gimlin, R. Burton, G. Hawkins, J. Mather, J. Rusek, F. Holcomb, Proceeding of Eighth International Hydrogen Peroxide Propulsion Conference, Purdue University, Lafayette, IN, USA, September 18–21, 2005, pp. 87–96.
[6] G.H. Miley, N. Luo, P.J. Shrestha, R. Gimlin, R. Burton, J. Rusek, F. Holcomb, AIAA International Energy Conversion Conference, San Francisco, August 2004.
[7] N. Luo, G.H. Miley, J. Mather, R. Burton, G. Hawkins, R. Gimlin, J. Rusek, T.I. Valdez, S.R. Narayanan, AIP Conference Proceedings, STAIF 2006, Albuquerque, New Mexico, February 2006, pp. 209–221.
[8] G.H. Miley, N. Luo, J. Mather, R. Burton, G. Hawkins, L. Gu, E. Byrd, R. Gimlin, P.J. Shrestha, G. Benavides, J. Laystrom, D. Carroll, J. Power Sources 165 (2007) 509–516.
[9] S. Amendola, P. Onnerud, M. Kelly, P. Petillo, S. Sharp Goldman, M. Binder, J. Power Sources 84 (1999) 130–133.
[10] M. Atwan, C.L.B. Macdonald, D.O. Northwood, E.L. Gyengec, J. Power Sources 158 (2006) 36–44.
[11] Z.P. Li, B.H. Liu, J.K. Zhu, S. Suda, J. Power Sources 163 (2006) 555–559.
[12] R.K. Raman, S.K. Prashant, A.K. Shukla, J. Power Sources 162 (2006) 1073–1076.
[13] M. Pourbaix, Atlas of Electrochemical Equilibria in Aqueous Solutions, Pergamon Press, Oxford, New York, 1966.
[14] W.F. Coleman, http://www.wellesley.edu/Chemistry/chem20/pour.html, 2003.
[15] W.X. Chen, J.Y. Lee, Z.L. Liu, Chem. Commun. 21 (2002) 2588.
[16] T.S. Armadi, Z.L. Wang, T.C. Green, A. Henglein, M.A. El-Sayed, Science 272 (1996) 1924–1925.
[17] X. Li, S. Ge, C.L. Hui, I.-M. Hsing, Electrochem. Solid-State Lett. 7 (9) (2004) A286–A289.
[18] V. Ganesh, D. Vijayaraghavan, V. Lakshminarayanan, Appl. Surf. Sci. 240 (2005) 286–295.
[19] X. Cheng, B. Yi, M. Han, J. Zhang, Y. Qiao, J. Yu, J. Power Sources 79 (1999) 75–81.
[20] N.A. Choudhury, R.K. Raman, S. Sampath, A.K. Shukla, J. Power Sources 143 (2005) 1–8.
[21] K.H. Choi, H.S. Kim, T.H. Lee, J. Power Sources 75 (1998) 230–235.
[22] D.K. Ivanou, E.A. Streltsov, A.K. Fedotov, A.V. Mazanik, D. Fink, A. Petrov, Thin Solid Films 490 (2005) 154–160.
[23] S. Hirano, J. Kim, S. Srinivasanl, Electrochim. Acta 42 (1997) 1587.
[24] D. Gruber, N. Ponath, J. Muller, F. Lindstaedt, J. Power Sources 150 (2005) 67–72.
[25] S. Litster, G. Mclean, J. Power Sources 130 (2004) 61–76.
[26] R. O'Hayre, S.J. Lee, S.W. Cha, F.B. Prinz, J. Power Sources 109 (2002) 483–493.